Carbohydrate Polymers 157 (2017) 429–437

Contents lists available at ScienceDirect

Carbohydrate Polymers

journal homepage: www.elsevier.com/locate/carbpol

A hierarchically porous cellulose monolith: A template-free fabricated, morphology-tunable, and easily functionalizable platform

Yuanrong Xin[a,b], Qiancheng Xiong[c], Qiuhong Bai[c], Miwa Miyamoto[a], Cong Li[c], Yehua Shen[c], Hiroshi Uyama[a,c,*]

[a] Department of Applied Chemistry, Graduate School of Engineering, Osaka University, Suita 565-0871, Japan
[b] School of Pharmacy, Jiangsu University, Zhenjiang, 212013, China
[c] Key Laboratory of Synthetic and Natural Functional Molecule Chemistry of Ministry of Education, College of Chemistry and Materials Science, Northwest University, Xi'an 710127, Shaanxi Province, China

ARTICLE INFO

Article history:
Received 9 August 2016
Received in revised form
20 September 2016
Accepted 4 October 2016
Available online 5 October 2016

Keywords:
Cellulose
Hierarchical structure
Tunable porous morphology
Monolith
Thermally induced phase separation

ABSTRACT

Recently, monoliths with continuous porous structure have received much attention for high-performance separation/adsorption matrix in biomedical and environmental fields. This study proposes a novel route to prepare cellulose monoliths with hierarchically porous structure by selecting cellulose acetate (CA) as the starting material. Thermally induced phase separation of CA solution using a mixed solvent affords a CA monolith, which is converted into the cellulose monolith by alkaline hydrolysis. Scanning electron microscopy images of the CA and cellulose monoliths reveal a continuous macropore with rough surface, and nitrogen adsorption/desorption analysis indicates the formation of a mesoporous structure. The macroporous structure could be controlled by changing the fabrication parameters. A series of reactive groups are introduced by chemical modifications on the surface of the cellulose monolith. The facile and diverse modifiability combined with its hydrophilic property make the hierarchically porous cellulose monolith a potential platform for use in separation, purification and bio-related applications.

1. Introduction

Hierarchically porous monoliths with continuous macroporous structures and large surface areas based on mesopores (Chakraborty, Colón, Snurr, & Ngugen, 2015; Moitra et al., 2013; Saba, Mousavi, Bühlmann, & Hillmyer, 2015; Sai et al., 2013; Ungureanu et al., 2015) can meet the demands of growing applications such as protein immobilization, adsorption, ion-exchange, catalysis, and sensors (Bronstein et al., 2004; Li, Tolley, & Lee, 2010; Okada, Asakura, Tokudome, Nakahira, & Takahashi, 2015; Tokarev, & Minko, 2009). The fabrication of such monoliths as well as control of the porous morphology for size-selective separation have been reported. Among these studies, there have been many reports on inorganic materials such as carbon, silica, and titanium dioxide (Inayat, Reinhardt, Uhlig, Einicke, & Enke, 2013; Moitra et al., 2013; Ungureanu et al., 2015). Although synthetic polymeric monoliths have been recently developed because of their excellent biocompatibility, high chemical stability, and facile modifiability (Nischang, & Causon, 2016; Nischang, 2013), fabrication techniques aiming to obtain hierarchically porous structures remains limited. In most cases, free-radical polymerization, polymerization of high internal phase emulsions, and thin-layer membrane fabrication are used (Bolton, Bailey, & Rzayev, 2011; Hess et al., 2015; Seo, Kim, Oh, Kim, & Hillmyer, 2015; Sevšek, Brus, Jeřabek, & Krajnc, 2014), which involve complicated and time-consuming processes.

We have achieved facile fabrication of hierarchically porous monoliths from polymer solutions using thermally induced phase separation (TIPS). Monoliths of poly(acrylonitrile), poly(vinyl alcohol), poly(ethylene-co-vinyl alcohol), and poly(γ-glutamic acid) were successfully prepared by selecting an appropriate mixed solvent (Okada et al., 2011; Park et al., 2013; Sun, Fujimoto, & Uyama, 2013; Wang, & Uyama, 2015). These monoliths contained uniform mesopores as well as sub-micron or micron-sized macropores. The monoliths were obtained using simple processes, namely, solubilization of the polymer powder into a mixture of solvents by heating and subsequent cooling of the solution, during which phase separation took place to form the monolith.

Cellulose, which is the most abundant organic compound on Earth, has a linear structure of a β(1 → 4) linked D-glucose repeating unit. It is one of the three major structural components of the primary cell walls of green plants, along with hemi-cellulose and

* Corresponding author at: Department of Applied Chemistry, Graduate School of Engineering, Osaka University, Suita 565-0871, Japan.
E-mail address: uyama@chem.eng.osaka-u.ac.jp (H. Uyama).

http://dx.doi.org/10.1016/j.carbpol.2016.10.006
0144-8617/

lignin. Based on its characteristic structure, cellulose possesses high crystallinity and mechanical strength. Additionally, cellulose is not soluble in water or common organic solvents due to the strong intermolecular hydrogen bonding of cellulose chains. In addition to the paper industry, cellulose is widely used in various fields such as the chemical, textile, and food industries. Furthermore, cellulose is one of the most important matrices for separation applications because of its high hydrophilicity, resistance to solvents, and mechanical strength (Credou, & Berthelot, 2014; Klemm, Heublein, Fink, & Bohn, 2005; Moon, Martini, Nairn, Simonsen, & Youngblood, 2011). In particular, its highly hydrophilic property prevents non-specific adsorption of biomolecules such as proteins on the cellulose matrix for biomedical applications.

Cellulose cannot be manufactured by melt processing techniques or casting method in common solvents. Therefore, good solvents for cellulose have been developed mainly for the production of cellulose fibers. A typical example is *N*-methylmorpholine-*N*-oxide monohydrate, which is used for the wet spinning of cellulose to prepare lyocell, one type of regenerated cellulose fiber (Fink, Ganster, & Lehmann, 2014; Fink, Weigel, Purz, & Ganster, 2001). In addition to this solvent, lithium chloride/*N*,*N*-dimethylacetamide (Chen et al., 2015; Zhang, Azuma, & Uyama, 2015; Zhang et al., 2014), NaOH/water (Budtova, & Navard, 2016), NaOH or LiOH/urea/water (Cai, Kimura, Wada, Kuga, & Zhang, 2008; Chang, Zhang, Zhou, Zhang, & Kennedy, 2010; Yang, Wu, Saito, & Isogai, 2014), $Ca(SCN)_2$/water (Hattori, Koga, Shimaya, & Saito, 1998), and ionic liquids (Abushammala, Krossing, & Laborie, 2015; Badgujar & Bhanage, 2015; Raut et al., 2015; Zhu et al., 2006) have been reported to solubilize cellulose.

The solubilization of cellulose has enabled the use of various processing procedures to prepare cellulose fibers, non-woven mats, gels, particles, membranes, films, and porous materials (Carrillo, Laine, & Rojas, 2014; Gericke, Trygg, & Fardim, 2013; Hosoda, Tsujimoto, & Uyama, 2014; Joshi et al., 2016; Nguyen et al., 2013; Wang, Lu, & Zhang, 2016). Highly porous cellulose beads have been obtained through dissolution in an ionic liquid (1-allyl-3-methlimidozoium chloride) and subsequent precipitation in a coagulation bath of ultrapure water. A calcium thiocyanate tetrahydrate/water/ethanol system was also employed to dissolve cellulose, and the production of a cellulose aerogel was achieved through a supercritical drying process. An amorphous transparent film of cellulose was also prepared from a lithium chloride/*N*,*N*-dimethylacetamide solution.

Porous cellulose materials such as cellulose aerogels and cellulose monoliths are useful as separation matrices in biomedical applications. The cellulose gel is prepared by a freeze-thaw process of a NaOH/urea/water solution followed by immersion in ethanol. This gel is converted into the cellulose aerogel by freeze drying or supercritical drying. Porous cellulose is also prepared from cellulose gel in LiOH/urea/water and $Ca(SCN)_2$/water. However, these methods have several drawbacks such as the use of toxic chemicals, high cost, and tedious procedures. Additionally, freeze drying or supercritical drying are often required for isolation of the porous cellulose materials, which is also unsuitable for industrial applications due to the high cost and energy use.

Cellulose acetate (CA) is one of the most important cellulose derivatives in the chemical industry. Two types of CA with different acetylation ratios, cellulose diacetate and cellulose triacetate, are industrially manufactured. The former is mainly used for fibers and the latter for films and sheets, which are widely employed as the polarizing plates of liquid crystal displays. These cellulose acetate derivatives are readily soluble in various organic solvents (Edgar et al., 2001; Konwarh, Karak, & Misra, 2013).

This study provides a new convenient route to prepare a cellulose monolith with hierarchically porous structure using CA as the starting material. The CA monolith was fabricated from its solution through TIPS, which was easily hydrolyzed to convert the cellulose monolith which exhibits high tolerance toward common solvents. Two steps were required for this route; however, each step contained a simple and convenient process. Therefore, the tedious and time-consuming processes were not involved due to avoiding cellulose as the starting material; also, the special isolation equipment for freeze drying or supercritical drying was not required. Furthermore, some reactive cellulose-based monoliths were developed by functionalization of the surface of the cellulose monolith.

2. Experimental section

2.1. Materials

Two types of commercially available CA with different molecular weights (CA1, CA2) were used in this work: CA1 ($M_n = 3.0 \times 10^4$; 39.3–40.3 wt% acetyl content); CA2 ($M_n = 5.0 \times 10^4$; 39.2–40.2 wt% acetyl content). These samples were purchased from Sigma-Aldrich Co. Picrylsulfonic acid solution (TNBS, 5% (w/v) in H_2O), *t*-butyl carbazate (TBC), and trichloroacetic acid (TCA) were also bought from Sigma-Aldrich Co. Sodium hydroxide (NaOH), potassium hydroxide (KOH), epichlorohydrin (EC), sodium thiosulfate, (*N*,*N*-dimethylformide) DMF, 1-hexanol, ethanol, hydrochloric acid solution (HCl; 0.01, 0.5, and 1.0 M), and methanol were obtained from Wako Pure Chemical Industries, Ltd. 1,2-Bis(2-aminoethoxy)ethane (BAE) and borate buffers (pH = 8.0 and 9.0) were supplied from Tokyo Chemical Industry Co. Ltd. All the reagents were used as received without further purification.

2.2. Measurements

Fourier-transform infrared (FT-IR) spectroscopy measurements using the attenuated total reflectance (ATR) method were performed by a Thermo Scientific Nicolet iS5 with iD5 ATR accessory. Nitrogen adsorption/desorption isotherms were measured with a NOVA 4200e surface area & pore size analyzer (Quantachrome Instruments) at 77 K. Before the measurements, the sample was degassed at room temperature under vacuum for at least 6 h. The specific surface area was calculated using the Brunauer–Emmett–Teller (BET) equation. Scanning electron microscopy (SEM) images were recorded by a Hitachi S-3000N instrument at 15 kV. A thin gold film was sputtered on the samples before the images were collected. X-ray diffraction (XRD) spectra were obtained on a Shimadzu XRD-6100 at a scanning rate of 4.0 °/min from 5 to 40° (2θ) at 40 kV and 30 mA using CuKα radiation. UV–vis absorbance measurements were carried out using a Hitachi U-2810 UV–vis spectrometer.

2.3. Fabrication of CA monolith

The typical fabrication protocol of the CA monolith was as follows (Fig. 1). First, CA powder (0.20 g) was completely dissolved in DMF (1.0 mL) at room temperature. 1-Hexanol (1.5 mL) was added dropwise into the solution with gentle stirring. The mixture was then heated at 70 °C until it became transparent. The solution was then maintained at 20 °C for 24 h to complete the phase separation. The solvent was replaced with ethanol three times and subsequently dried in vacuo to furnish the CA monolith.

2.4. Fabrication of cellulose monolith

The cellulose monolith was obtained through the hydrolysis of the CA monolith (Fig. 1). The CA monolith (50 mg) was first immersed in 2.0 mL of methanol. After degassing for 5 min, 0.15 mL of 2 M NaOH solution in methanol was added to start the hydrolysis

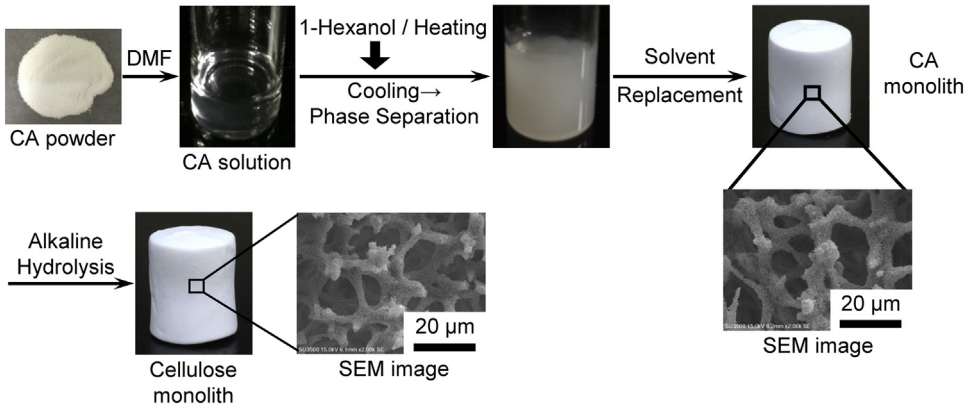

Fig. 1. Fabrication process of cellulose monolith.

reaction at room temperature. After 3 h, the solution was neutralized with 1 M HCl. The hydrolyzed cellulose monolith was rinsed with water and methanol successively and dried in vacuo.

2.5. Synthesis of epoxy-modified cellulose monolith (ECL monolith)

The cellulose monolith (0.50 g) was first soaked with water and immersed into 0.1 mL of 10 wt% aqueous NaOH solution. The mixture was kept for 1 h at 30 °C under gentle shaking. Subsequently, 0.4 mL of EC was added, and the reaction was performed for an additional 2 h at 30 °C. The ECL monolith was washed thoroughly with water until the eluate became neutral and then dried in vacuo. The amount of the epoxy group functionalized on the surface of the ECL monolith was determined based on the reaction with sodium thiosulfate and titration of the released OH^- by 0.01 M HCl (Sundberg & Porath, 1974).

2.6. Synthesis of amine-functionalized cellulose monolith (AMCL monolith)

The ECL monolith (50 mg) was mixed with 1.0 mL of 0.7 mM BAE aqueous solution. The reaction was carried out for 24 h at 45 °C. The resultant AMCL monolith was thoroughly washed with water until the eluate became neutral and was then dried in vacuo. The amount of the primary amine group located on the surface of the AMCL monolith was determined through a modified TNBS method, which was performed through the reaction between the primary amine group and TNBS, and the absorbance measurement after the subsequent alkaline hydrolysis (Snyder & Sobocinski, 1975).

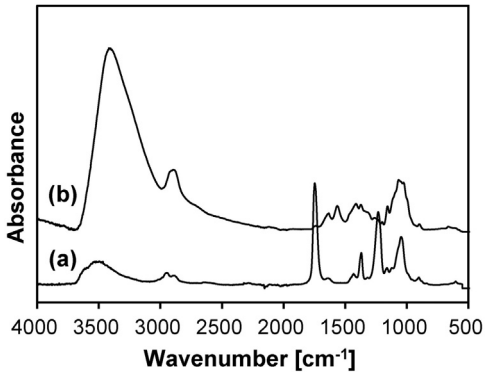

Fig. 2. FT-IR spectra of (a) CA monolith and (b) cellulose monolith.

2.7. Synthesis of aldehyde-activated cellulose monolith (AHCL monolith)

The AMCL monolith (0.50 g) was immersed into 1.9 mL of 25 wt% glutaraldehyde solution, and the reaction was performed for 4 h at 40 °C with gentle stirring. The activated monolith was rinsed thoroughly with distilled water and dried in vacuo. The amount of the aldehyde group in the AHCL monolith was quantified using the reaction with TBC to form stable carbazone and the absorbance

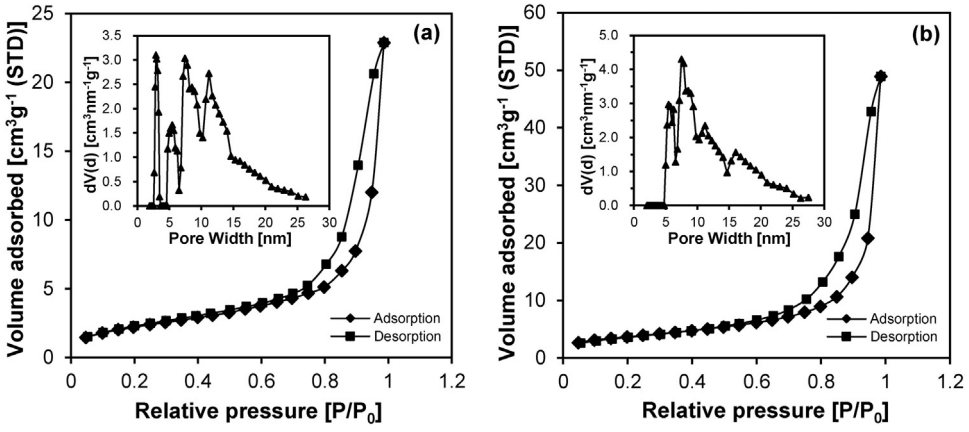

Fig. 3. Nitrogen adsorption/desorption isotherms of (a) CA monolith and (b) cellulose monolith. Inset: pore size distribution plots of CA and cellulose monolith.

measurement after reacting with TNBS for determination of unreacted TBC (Bouhadir, Hausman, & Mooney, 1999).

3. Results and discussion

3.1. Fabrication and characterization of cellulose monolith

Solvent selection is often a crucial factor in fabricating polymer monoliths by TIPS. In this study, cellulose diacetate was used as the starting material because its solubility toward organic solvents is superior to that of cellulose triacetate. The cellulose diacetate, abbreviated here as CA, was soluble in acetone, tetrahydrofuran, DMF, *N*,*N*-dimethylacetamide, dimethylsulfoxide, and *N*-methypyrrolidone. Concerning the TIPS process, acetone and tetrahydrofuran have low boiling temperatures, which restricts the phase separation condition upon heating; thus, DMF was selected as a good solvent for the fabrication of the CA monolith. The non-solvents of CA, the vital factor determining the monolith morphology, were screened to form the CA monolith under appropriate phase separation conditions, and the selection of 1-hexanol with the mixed ratio of 1-hexanol/DMF = 1/1.5 (v/v) was observed to provide the CA monolith with good columnar shape (Fig. 1). SEM observation revealed the three-dimensional (3D) open pore structure. The average skeleton size was approximately 3.6 μm.

Hydrolysis of CA was carried out using NaOH in methanol at room temperature. The resulting monolith was insoluble in water and common organic solvents such as ethanol, chloroform, DMF, DMAc, DMSO, and toluene. Fig. 2 represents the FT-IR spectra of the monolith before and after the hydrolysis. The strong characteristic peak at 1740 cm^{-1} due to the stretching vibration of C═O of the acetyl group completely disappeared in the spectrum after the hydrolysis. Additionally, the broad absorbance peak at 3200–3680 cm^{-1} due to the stretching vibration of O—H became much larger after the hydrolysis. The spectrum after the hydrolysis was in good accordance with that of reagent cellulose. These data clearly suggest that the acetyl group of CA was selectively hydrolyzed under the present conditions. The cleavage of the main chain of CA may occur by alkaline hydrolysis; however, the use of methanol as a solvent under mild reaction conditions enabled the selective hydrolysis of the side chain in CA. After the hydrolysis, the monolith shape and morphology were retained (Fig. 1).

The nitrogen adsorption/desorption isotherms for the CA and cellulose monoliths reveal a type V isotherms with relatively wide type H1 hysteresis loops in the P/P_0 range from 0.3 to 1.0 and 0.5 to 1.0, respectively (Fig. 3). A type V isotherm is characteristic of a material with mesoporosity and low energy of adsorption; it often contains hysteresis attributed to the mesoporosity. Using the non-local density functional theory (NLDFT) method, pore size distribution (PSD) plots for the CA and cellulose monoliths were obtained, which revealed uniform pores with diameters of 7.8 and 11.2 nm. The specific surface areas of the CA and cellulose monoliths were calculated to be 41.3 and 42.3 $m^2\ g^{-1}$, respectively, by the multi-point BET equation. These data indicate the formation of hierarchically porous structures with relatively uniform mesopores in the CA and cellulose monoliths. XRD analysis of the cellulose monolith showed an amorphous structure; a broad peak was observed at 2θ = 5 to 30° (Fig. S1).

To understand the formation of the spectacular hierarchical structure inside the fabricated cellulose monolith, the following hypothesis is proposed. The CA solution heated at 70 °C gradually becomes unstable when it is cooled at the standing temperature (20 °C) due to the binodal or spinodal decompositions according to the corresponding fabrication parameters. Here, the TIPS of the CA solution begins, and the entire process can be divided into two steps concluding with liquid–liquid (L–L) and solid–liquid (S–L, polymer crystallization) phase separations, which is the key factor in generating the hierarchical structure. In the present case, the compatibility between the CA polymer and mixture solvent system (DMF/1-hexanol) is relatively poor, leading to the low crystallization temperature, which is below the binodal line.

Initially, the solubility of the mixed solvent system drops due to the decrease of temperature. To reduce the overall Gibbs free energy according to the second law of thermodynamics, L–L phase separation is induced, resulting in a polymer-rich and polymer-lean phase. The polymer-rich phase develops in the form of a monolith with the formation of a continuous matrix, while the polymer-lean phase mainly consisting of the solvent mixture flows through the matrix to bring the porous channels within the monolith.

During this stage, the CA polymer chains can easily orient and arrange orderly due to the chain movement to the polymer-rich phase. As the temperature is further reduced, ordering and/or stretching of the CA polymer chains may take place to achieve sufficient regularity and easily arrange into the crystalline lattice, inducing the nucleation and crystallization of CA while simultaneously generating the S-L phase separation. This crystallization-induction phenomenon was also observed in the formation of a polycarbonate monolith using non-solvent induced phase separation (Xin, Fujimoto, & Uyama, 2012).

Due to the interconnection of these crystalline particles formed inside the polymer-rich phase, the spaces generated between them lead to the mesopores. Together with the macropores between the polymer-rich and polymer-lean phase in the process of L–L phase separation, the hierarchical structure is obtained for the CA monolith without any templating.

Subsequently, after the mild hydrolysis reaction, the hierarchically porous morphology survives inside the resultant cellulose monolith even though the crystallization lattice is destroyed because of the loss of acetate ester groups. Inside the cellulose monolith, the macroporous structure supplies sufficient space for the rapid flowing of large bio-related molecules; on the other hand, the mesoporous structure, resulting in the large surface area, can increase the mass permeability. Therefore, the fabricated cellulose monolith with hierarchically porous structure is an ideal candidate for the stationary phase of columns in separation and purification applications.

3.2. Morphology control of monolith

The effects of various fabrication parameters on the morphology of the CA monolith were systematically investigated. First, the polymer concentration was examined to elaborate the mechanism of the morphology control in the CA monolith. Fig. 4 presents SEM images of the CA and cellulose monoliths prepared with different CA concentrations. The molecular weight of CA and the mixed ratio of 1-hexanol/DMF were 5.0×10^4 and 1.5/1 (v/v), respectively. For the 150 mg mL^{-1} concentration, the particle-connected morphology was found, whereas the columnar skeleton was observed for the 200 mg mL^{-1} concentration. In the former case, due to the lower CA concentration, the phase separation point in the polymer phase diagram might be located between the binodal and spinodal curves, which is the metastable area. In this case, the fewer CA polymer chains existing in the solution hardly have the opportunity to contact with each other and therefore can only form the globular-like morphology after the accomplishment of the phase separation following the nucleation and growth mechanism. However, the phase separation point for the higher CA polymer concentration would be located in the unstable region, which is below the spinodal curve. Due to the higher concentration, the CA solution contains relatively more polymer chains favorable for easily interconnected tangling, leading to growth into a well-interconnected open porous columnar morphology and facilitating the eventual formation of

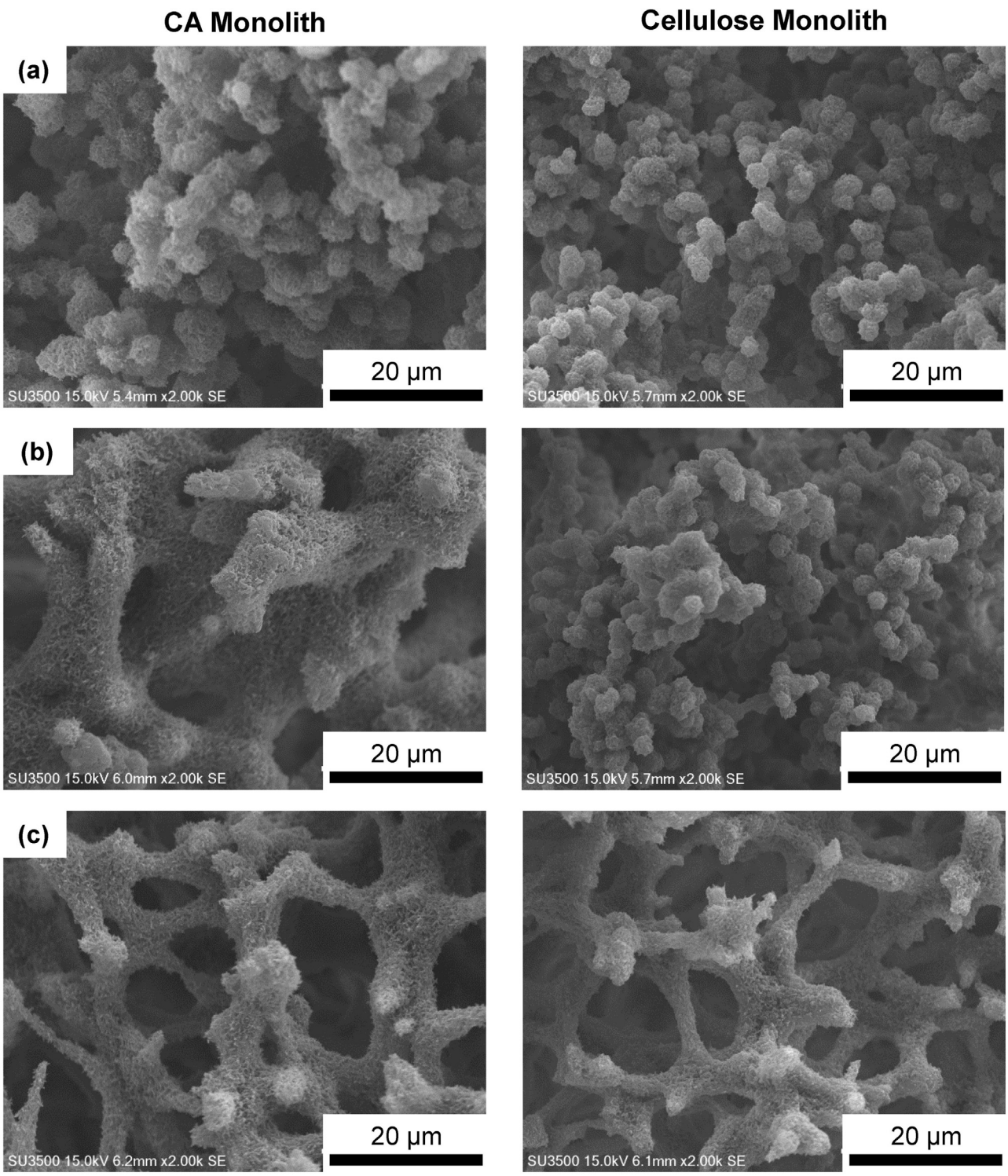

Fig. 4. SEM images of CA and cellulose monoliths with CA concentration of (a) 150 mg mL^{-1}, (b) 180 mg mL^{-1}, and (c) 200 mg mL^{-1} (molecular weight of CA: 5.0×10^4; 1-hexanol/DMF: 1.5/1 (v/v)).

a 3D continuous skeletal structure, which is in agreement with the spinodal decomposition mechanism. Despite the dissimilarities of CA monoliths with different polymer concentration, the porous structure of corresponding cellulose monoliths remained after the alkaline hydrolysis. Except for the monolith with CA concentration of 180 mg/mL, the morphology was almost the same as that before the hydrolysis.

The effect of the molecular weight of CA on the morphology of the monolith is shown in Fig. 5. Two kinds of CA (CA1 and CA2) with molecular weights of 3.0×10^4 and 5.0×10^4 were used. The CA concentration and mixed ratio of 1-hexanol/DMF were 200 mg mL^{-1} and 1.5/1 (v/v), respectively. In both cases, the monolith possessed a relatively uniform structure, and a rough skeleton surface was observed. The molecular weight of CA was also observed to significantly affect the inner morphology of the resultant mono-

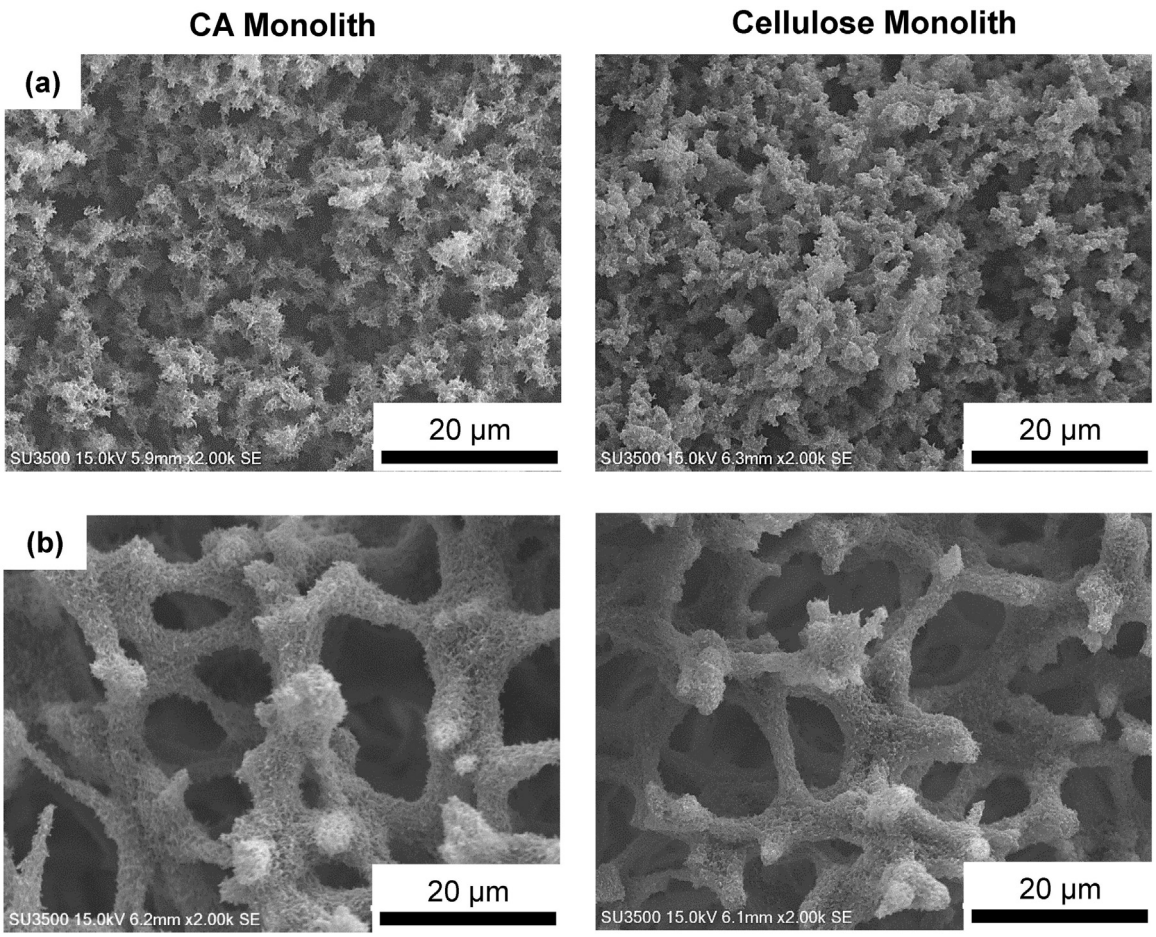

Fig. 5. SEM images of CA and cellulose monoliths with molecular weight of (a) 3.0×10^4 and (b) 5.0×10^4 (CA concentration: 200 mg mL^{-1}; 1-hexanol/DMF: 1.5/1 (v/v)).

lith. The CA1 monolith with lower molecular weight possessed a particulate-like structure, whereas the CA2 monolith possessed a clear 3D interconnected skeletal structure. The reason for the morphology difference is similar to that of the effect of the polymer concentration. This phenomenon might be interpreted as follows. During the phase separation process, the CA polymer chains tend to aggregate to form nuclei due to the low solubility toward the mixture solvent used. For the CA with higher molecular weight, the longer polymer chains could interconnect and entangle with the neighbor ones more easily and grow into the 3D skeletal structure. The morphology of the cellulose monolith obtained by the alkaline hydrolysis was similar to that before the hydrolysis, whereas its skeleton size slightly decreased.

The composition of the mixed solvent greatly affected the monolith morphology (Fig. 6). To examine the solvent composition, the molecular weight of CA and the mixed ratio of 1-hexanol/DMF were fixed at 5.0×10^4 and 1.5/1 (v/v), respectively. The ratio of 1-hexanol to DMF changed from 1.5 to 2. As the ratio increased, the skeleton size decreased because the phase separation occurred faster in the solvent with the higher content of the non-solvent for CA. Below the ratio of 1.5, phase separation did not take place, and above the ratio of 2.0, the polymer was not completely soluble in the mixed solvent on heating. For all the cases, the CA monolith could be converted into the cellulose monolith with the decrease of the skeleton size.

These data strongly suggest that the skeleton size and inner morphology of the CA monolith could be tuned by changing the phase separation parameters (polymer concentration, molecular weight of CA, and solvent composition). Additionally, the resulting CA monolith was successfully converted into the cellulose monolith for all the cases examined and the porous morphology hardly changed after the hydrolysis.

3.3. Introduction of reactive groups on cellulose monolith

Many cellulose derivatives have been prepared, and some of them, typically, CA, carboxymethyl cellulose, methyl cellulose, and hydroxyethyl cellulose, are widely used in various industries. A variety of functional groups have been reported to be introduced at the hydroxyl groups of cellulose. Here, the introduction of typical reactive groups, epoxy, primary amine, and aldehyde, on the skeleton surface of the cellulose monolith was examined (Fig. 7).

An epoxy group was introduced via the reaction of the cellulose monolith with EC in NaOH solution. The epoxy content of the ECL monolith was determined to be 270 μmol g^{-1}. Subsequently, the ECL monolith was converted into the AMCL monolith by the reaction with a large excess of BAE in an aqueous solution, and the resultant amine content was 257 μmol g^{-1}, which was somewhat lower than the epoxy content. This lower content may be due to the partial crosslinking between the nearby epoxy groups by the amine group. The primary amine on the AMCL monolith was easily converted into an aldehyde group by the reaction with a large excess of glutaraldehyde, and the aldehyde content was 239 μmol g^{-1}. The methods employed to determine the corresponding functional groups are summarized in the Supporting information.

The introduction of these functional groups into the cellulose-based monolith were confirmed by FT-IR spectroscopy (Fig. S2). For the ECL monolith, the absorbance peak attributed to the stretching

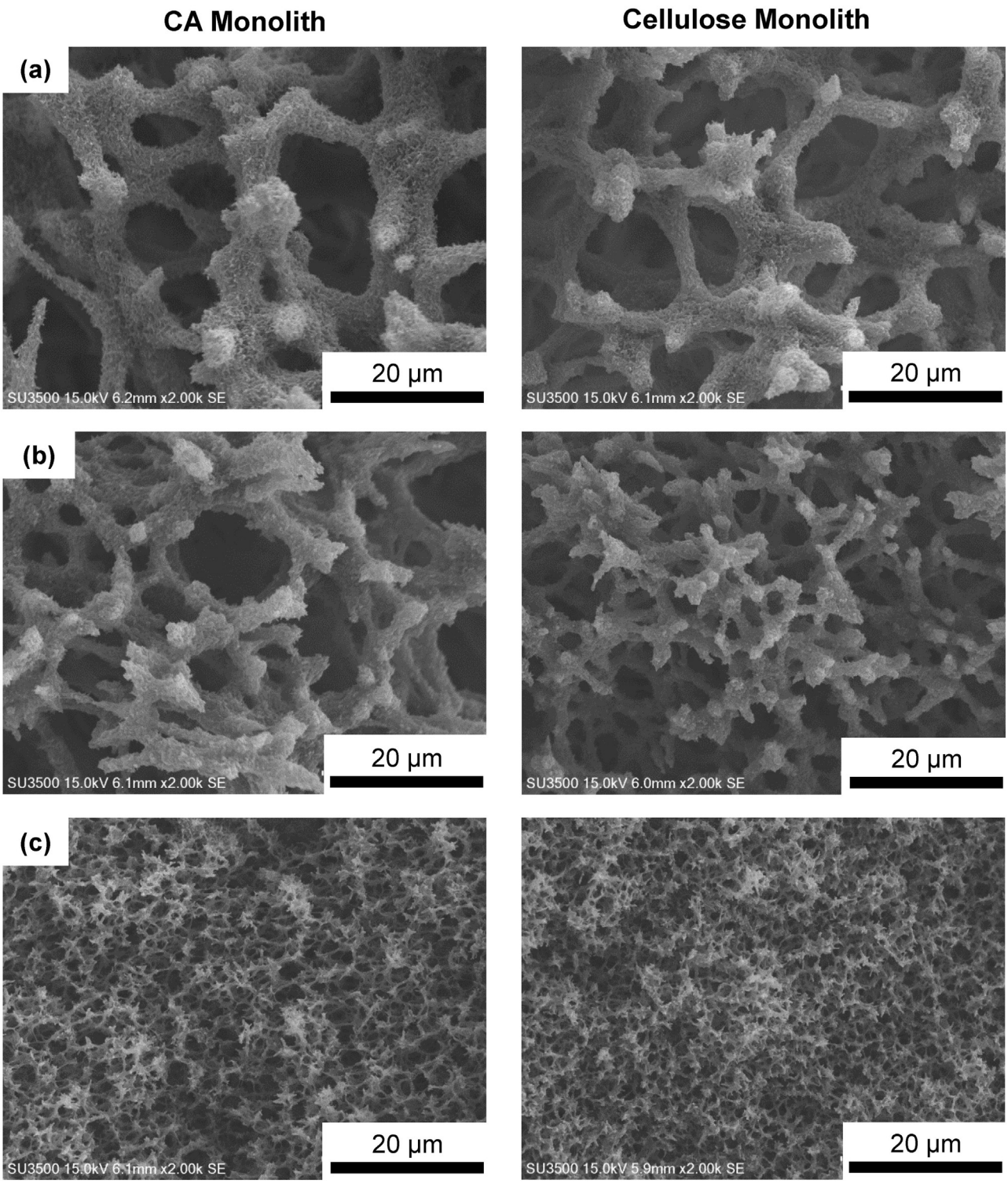

Fig. 6. SEM images of CA and cellulose monoliths with 1-hexanol/DMF ratio of (a) 1.5/1, (b) 1.75/1, and (c) 2/1 (molecular weight of CA: 5.0×10^4; CA concentration: 200 mg mL^{-1}).

vibration of O—H became much smaller compared with that of the cellulose monolith. Additionally, new peaks located at 1000, 1020, and 1150 cm^{-1} from the stretching vibration of C—OH and broad peaks at 806–871 and 907 cm^{-1} due to the epoxy ring vibration were observed in the spectrum of the ECL monolith (Fig. S2b). In the spectrum of the AMCL monolith (Fig. S2c), the absorbance peaks attributed to the epoxy ring disappeared after the reaction with BAE, supporting the introduction of the primary amine group. A characteristic peak at 1720 cm^{-1} due to the stretching vibration of the aldehyde group newly appeared in the FT-IR spectrum of the AHCL monolith (Fig. S2d). These results clearly demonstrate that the epoxy, primary amine, and aldehyde groups were successfully introduced on the skeleton surface of the cellulose monolith. These reactive groups are highly useful for immobilization of functional molecules on the cellulose monolith.

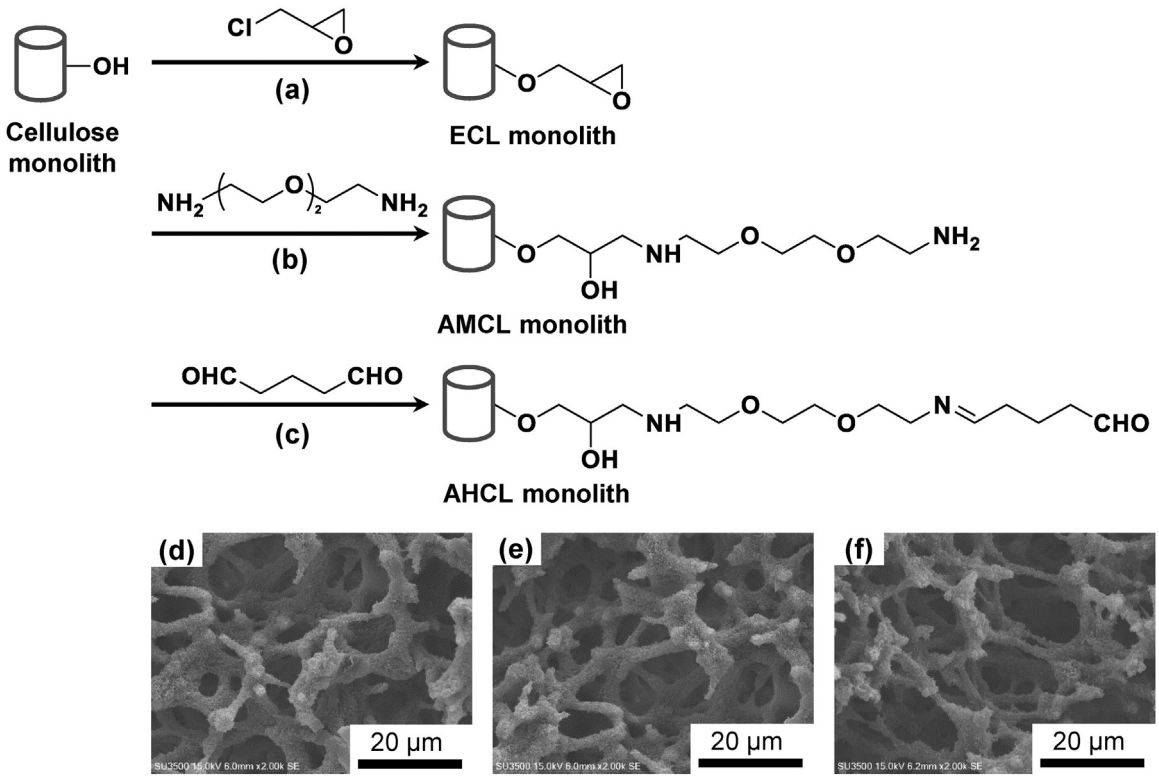

Fig. 7. Introduction of reactive (a) epoxy, (b) primary amine, and (c) aldehyde groups on cellulose monolith and the corresponding SEM images of (d) ECL, (e) AMCL and (f) AHCL monolith.

4. Conclusions

A hierarchically porous cellulose monolith exhibiting high hydrophilicity and tolerance toward common solvents was readily fabricated from a CA solution by TIPS. A mixed solvent of 1-hexanol and DMF in the appropriate mixed ratio provided the CA monolith with a 3D continuous macroporous structure in a columnar shape. BET analysis revealed the formation of a uniform mesopore of 11.2 nm. The phase separation parameters including the polymer concentration, molecular weight of CA, and ratio of 1-hexanol/DMF greatly affected the skeleton size and inner morphology of the CA monolith. The alkaline hydrolysis of the CA monolith in methanol selectively proceeded to give the cellulose monolith, and the shape and morphology hardly changed after the hydrolysis. Typical reactive groups, epoxy, primary amine, and aldehyde, were introduced on the skeleton surface of the cellulose monolith.

Cellulose-based matrices are useful for the separation of bio-related molecules such as antibodies, protein drugs, DNA, and SiRNA. Therefore, a variety of studies on fabrication techniques, shape and morphology control, and the introduction of ligands, have been extensively developed (Carrillo et al., 2014; Gericke et al., 2013; Hosoda et al., 2014; Joshi et al., 2016; Nguyen et al., 2013; Wang et al., 2016). The present cellulose monolith possessed several features such as easy chemical modification, high solvent efficient mass transfer, large surface area, high stability, and high mechanical strength as a result of the cmonolithic and hierarchically porous structure as well as characteristic properties of cellulose. Therefore, the cellulose monolith and its reactive derivatives have great potential for the efficient separation of bio-related molecules. Further studies on the fabrication and applications of protein-loading cellulose monoliths are currently in progress in our laboratory.

Acknowledgements

This study is financially supported by a Grant-in-Aid for Scientific Research from the Japan Society for the Promotion of Science (No. 25288090), a Project for Creating Start-ups from Advanced Research and Technology, MEXT, the Hundred Talents Program, Shaanxi Province, PR China, the Natural Science Foundation of Jiangsu Province for Youth (No. BK20160496) and the Scientific Research Foundation of Jiangsu University (No. 5501290002).

Appendix A. Supplementary data

Supplementary data associated with this article can be found, in the online version, at http://dx.doi.org/10.1016/j.carbpol.2016.10.006.

References

Abushammala, H., Krossing, I., & Laborie, M. P. (2015). Ionic liquid-mediated technology to produce cellulose nanocrystals directly from wood. *Carbohydrate Polymers*, *134*, 609–616.

Badgujar, K. C., & Bhanage, B. M. (2015). Factors governing dissolution process of lignocellulosic biomass in ionic liquid: Current status, overview and challenges. *Bioresource Technology*, *178*, 2–18.

Bolton, J., Bailey, T. S., & Rzayev, J. (2011). Large pore size nanoporous materials from the self-assembly of asymmetric bottlebrush block copolymers. *Nano Letters*, *11*, 998–1001.

Bouhadir, K. H., Hausman, D. S., & Mooney, D. J. (1999). Synthesis of cross-linked poly(aldehyde guluronate) hydrogels. *Polymer*, *40*, 3575–3584.

Bronstein, L. M., Goerigk, G., Kostylev, M., Pink, M., Khotina, I. A., Valetsky, P. M., et al. (2004). Structure and catalytic properties of Pt-modified hyper-cross-linked polystyrene exhibiting hierarchical porosity. *The Journal of Physical Chemistry B*, *108*, 18234–18242.

Budtova, T., & Navard, P. (2016). Cellulose in NaOH-water based solvents: A review. *Cellulose*, *23*, 5–55.

Cai, J., Kimura, S., Wada, M., Kuga, S., & Zhang, L. (2008). Cellulose aerogels from aqueous alkali hydroxide-urea solution. *ChemSusChem*, *1*, 149–154.

Carrillo, C. A., Laine, J., & Rojas, O. J. (2014). Microemulsion systems for fiber deconstruction into cellulose nanofibrils. *ACS Applied Materials & Interfaces*, *6*, 22622–22627.
Chakraborty, S., Colón, Y. J., Snurr, R. Q., & Nguyen, S. T. (2015). Hierarchically porous organic polymers: Highly enhanced gas uptake and transport through templated synthesis. *Chemical Science*, *6*, 384–389.
Chang, C., Zhang, L., Zhou, J., Zhang, L., & Kennedy, J. F. (2010). Structure and properties of hydrogels prepared from cellulose in NaOH/urea aqueous solutions. *Carbohydrate Polymers*, *82*, 122–127.
Chen, J., Guan, Y., Wang, K., Zhang, X., Xu, F., & Sun, R. (2015). Combined effects of raw materials and solvent systems on the preparation and properties of regenerated cellulose fibers. *Carbohydrate Polymers*, *128*, 147–153.
Credou, J., & Berthelot, T. (2014). Cellulose: From biocompatible to bioactive material. *Journal of Materials Chemistry B*, *2*, 4767–4788.
Edgar, K. J., Buchanan, C. M., Debenham, J. S., Rundquist, P. A., Seiler, B. D., Shelton, M. C., et al. (2001). Advances in cellulose ester performance and application. *Progress in Polymer Science*, *26*, 1605–1688.
Fink, H., Weigel, P., Purz, H. J., & Ganster, J. (2001). Structure formation of regenerated cellulose material from NMMO-solutions. *Progress in Polymer Science*, *26*, 1473–1524.
Fink, H., Ganster, J., & Lehmann, A. (2014). Progress in cellulose shaping: 20 years industrial case studies at Fraunhofer IAP. *Cellulose*, *21*, 31–51.
Gericke, M., Trygg, J., & Fardim, P. (2013). Functional cellulose beads: Preparation, characterization and applications. *Chemical Reviews*, *113*, 4812–4836.
Hattori, M., Koga, T., Shimaya, Y., & Saito, M. (1998). Aqueous calcium thiocyanate solution as a cellulose solvent. Structure and interactions with cellulose. *Polymer Journal*, *30*(1), 43–48.
Hess, S. C., Kohll, A. X., Raso, R. A., Schumacher, C. M., Grass, R. N., & Stark, W. J. (2015). Template-particle stabilized bicontinuous emulsion yielding controlled assembly of hierarchical high-flux filtration membranes. *ACS Applied Materials & Interfaces*, *7*, 611–617.
Hosoda, N., Tsujimoto, T., & Uyama, H. (2014). Green composite of poly(3-hydroxybutyrate-*co*-3-hydroxyhexanoate) reinforced with porous cellulose. *ACS Sustainable Chemistry & Engineering*, *2*, 248–253.
Inayat, A., Reinhardt, B., Uhlig, H., Einicke, W., & Enke, D. (2013). Silica monoliths with hierarchical porosity obtained from porous glasses. *Chemical Society Reviews*, *42*, 3753–3764.
Joshi, M. K., Pant, H. R., Tiwari, A. P., Maharjan, B., Liao, N., Kim, H. J., et al. (2016). Three-dimensional cellulose sponge: Fabrication, characterization, biomimetic mineralization, and in vitro cell infiltration. *Carbohydrate Polymers*, *136*, 154–162.
Klemm, D., Heublein, B., Fink, H., & Bohn, A. (2005). Cellulose: Fascinating biopolymer and sustainable raw material. *Angewandte Chemie International Edition*, *44*, 3358–3393.
Konwarh, R., Karak, N., & Misra, M. (2013). Electrospun cellulose acetate nanofibers: The present status and gamut of biotechnological applications. *Biotechnology Advances*, *31*, 421–437.
Li, Y., Tolley, H. D., & Lee, M. L. (2010). Size-exclusion separation of proteins using a biocompatible polymeric monolithic capillary column with mesoporosity. *Journal of Chromatography A*, *1217*, 8181–8185.
Moitra, N., Kanamori, K., Shimada, T., Takeda, K., Ikuhara, Y., Gao, X., et al. (2013). Synthesis of hierarchically porous hydrogen silsesquioxane monoliths and embedding of metal nanoparticels by on-site reduction. *Advanced Functional Materials*, *23*, 2714–2722.
Moon, R. J., Martini, A., Nairn, J., Simonsen, J., & Youngblood, J. (2011). Cellulose nanomaterials review: Structure, properties and nanocomposites. *Chemical Society Reviews*, *40*, 3941–3994.
Nguyen, S. T., Feng, J., Le, N. T., Le, A. T. T., Hoang, N., Tan, V. B. C., et al. (2013). Cellulose aerogel from paper waste for crude oil spill cleaning. *Industrial & Engineering Chemistry Research*, *52*, 18386–18391.
Nischang, I., & Causon, T. J. (2016). Porous polymer monoliths: From their fundamental structure to analytical engineering applications. *Trends in Analytical Chemistry*, *75*, 108–117.
Nischang, I. (2013). Porous polymer monoliths: Morphology, porous properties polymer nanoscale gel structure and their impact on chromatographic performance. *Journal of Chromatography A*, *1287*, 39–58.
Okada, K., Nandi, M., Maruyama, J., Oka, T., Tsujimoto, T., Kondoh, K., et al. (2011). Fabrication of mesoporous polymer monolith: A template-free approach. *Chemical Communications*, *47*, 7422–7424.
Okada, K., Asakura, G., Tokudome, Y., Nakahira, A., & Takahashi, M. (2015). Macroporous titanate nanotube/TiO_2 monolith for fast and large capacity cation exchange. *Chemistry of Materials*, *27*, 1885–1891.
Park, S., Fujimoto, T., Mizohata, E., Inoue, T., Sung, M., & Uyama, H. (2013). Fabrication of poly(γ-glutamic acid) monolith by thermally induced phase separation and its application. *Journal of Microbiology and Biotechnology*, *23*(7), 942–952.
Raut, D. G., Sundman, O., Su, W., Virtanen, P., Sugano, Y., Kordas, K., et al. (2015). A morpholinium ionic liquid for cellulose dissolution. *Carbohydrate Polymers*, *130*, 18–25.
Saba, S. A., Mousavi, M. P. S., Bühlmann, P., & Hillmyer, M. A. (2015). Hierarchically porous polymer monoliths by combining controlled macro- and microphase separation. *Journal of the American Chemical Society*, *137*, 8896–8899.
Sai, H., Tan, K. W., Hur, K., Asenath-Smith, E., Hovden, R., Jiang, Y., et al. (2013). Hierarchical porous polymer scaffolds from block copolymers. *Science*, *341*, 530–534.
Seo, M., Kim, S., Oh, J., Kim, S., & Hillmyer, M. A. (2015). Hierarchically porous polymers from hyper-cross-linked block polymer precursors. *Journal of the American Chemical Society*, *137*, 600–603.
Sevšek, U., Brus, J., Jeřabek, K., & Krajnc, P. (2014). Post polymerisation hypercrosslinking of styrene/divinylbenzene poly(HIPE)s: Creating micropores within macroporous polymer. *Polymer*, *55*, 410–415.
Snyder, S. L., & Sobocinski, P. Z. (1975). An improved 2,4,6-trinitrobenzenesulfonic acid method for the determination of amines. *Analytical Biochemistry*, *64*, 284–288.
Sun, X., Fujimoto, T., & Uyama, H. (2013). Fabrication of a poly(vinyl alcohol) monolith via thermally impacted non-solvent-induced phase separation. *Polymer Journal*, *45*, 1101–1106.
Sundberg, L., & Porath, J. (1974). Preparation of adsorbents for biospecific affinity chromatography: I. Attachment of group-containing ligands to insoluble polymers by means of bifunctional oxiranes. *Journal of Chromatography*, *90*, 87–98.
Tokarev, I., & Minko, S. (2009). Multiresponsive, hierarchically structured membranes: New, challenging, biomimetic materials for biosensors, controlled release, biochemical gates and nanoreactors. *Advanced Materials*, *21*, 241–247.
Ungureanu, S., Birot, M., Deleuze, H., Schmitt, V., Mano, N., & Backov, R. (2015). Triple hierarchical micro-meso-macroporous carbonaceous foams bearing highly monodisperse macroporosity. *Carbon*, *91*, 311–320.
Wang, G., & Uyama, H. (2015). Reactive poly(ethylene-*co*-vinyl alcohol) monoliths with tunable pore morphology for enzyme immobilization. *Colloid and Polymer Science*, *293*, 2429–2435.
Wang, S., Lu, A., & Zhang, L. (2016). Recent advances in regenerated cellulose materials. *Progress in Polymer Science*, *53*, 169–206.
Xin, Y., Fujimoto, T., & Uyama, H. (2012). Facile fabrication of polycarbonate monolith by non-solvent induced phase separation method. *Polymer*, *53*, 2847–2853.
Yang, Q., Wu, C., Saito, T., & Isogai, A. (2014). Cellulose-clay layered nanocomposite films fabricated from aqueous cellulose/LiOH/urea solution. *Carbohydrate Polymers*, *100*, 179–184.
Zhang, C., Liu, R., Xiang, J., Kang, H., Liu, Z., & Huang, Y. (2014). Dissolution mechanism of cellulose in *N*,*N*-dimethylacetamide/lithium chloride: Revisiting through molecular interactions. *The Journal of Physical Chemistry B*, *118*, 9507–9514.
Zhang, B., Azuma, J., & Uyama, H. (2015). Preparation and characterization of a transparent amorphous cellulose film. *RSC Advances*, *5*, 2900–2907.
Zhu, S., Wu, Y., Chen, Q., Yu, Z., Wang, C., Jin, S., et al. (2006). Dissolution of cellulose with ionic liquids and its application: A mini-review. *Green Chemistry*, *8*, 325–327.